Stochastic and Deterministic Vector Chromatography of Suspended Particles in One-Dimensional Periodic Potentials

Jorge A. Bernate* and German Drazer†

Department of Chemical and Biomolecular Engineering, Johns Hopkins University, Baltimore, Maryland 21218, USA

(Received 12 October 2011; published 21 May 2012)

We present a comprehensive description of vector chromatography (VC) that includes deterministic and stochastic transport in one-dimensional periodic free-energy landscapes, with both energetic and entropic contributions, and identifies the parameters governing the deflection angle. We also investigate the dependence of the deflection angle on the shape of the free-energy landscape by varying the width of the linear transitions in an otherwise dichotomous potential. Finally, we present experimental results obtained in a microfluidic system in which gravity drives the suspended particles and, in combination with a bottom surface patterned with shallow rectangular grooves, creates a periodic landscape of (potential) energy barriers. The experiments validate the model and demonstrate that a simple, passive microdevice can lead to VC of colloidal particles based on both size and density. More generally, other fields, e.g., electric, dielectrophoretic, or magnetic, can play or enhance the role of gravity, potentially leading to a versatile technique.

DOI: 10.1103/PhysRevLett.108.214501 PACS numbers: 47.61.Jd, 05.10.Gg, 05.40.−a

Micro- and nanofluidic systems for chemical and biological separation have shown great promise and opened the door for exciting new technologies. A number of separation systems based on driving suspended particles through a periodic stationary phase, for example, take advantage of the unprecedented control on the geometry and chemistry provided by available fabrication techniques. Driving suspended particles in one-dimensional (1D) periodic devices has been shown to lead to separation in a number of systems, ranging from entropic trap arrays [1] to ratchets based on asymmetric structures [2]. In addition, the 1D transport of particles past periodic entropy barriers and, to a lesser extent, energy barriers has received considerable attention, and rigorous results are available for the effective mobility of single particles [3–13]. Two-dimensional separation methods, in which different species in a sample migrate in different directions, enabling their continuous fractionation and, in general, providing greater selectivity than 1D techniques, have also been developed based on periodic stationary media and have been categorized as vector chromatography (VC) [14]. Notably, VC can be obtained in planar devices via a straightforward extension of the aforementioned 1D methods by driving the particles at an oblique angle with respect to the periodic direction, thus providing passive transport in the invariant direction. A representation of such systems is given in Fig. 1, including the case investigated in recent experiments in which suspended particles are driven through force fields that are periodic in one of the directions of the separation plane and invariant in the other [15–17]. Although a case-by-case analysis in the deterministic limit provided good agreement with these experiments, a general description is lacking. In this Letter, we present a comprehensive description of planar VC in terms of the 1D periodic free energy of the system, including energetic and entropic contributions, that captures the deterministic and Brownian limits. This unified description highlights the key parameters governing the migration angle of different species and their relevance to the design and optimization of fractionation devices. We also performed experiments in a microfluidic system in which gravity drives the particles and also, in combination with a patterned bottom surface, creates a periodic landscape of potential energy barriers. The experiments agree well with the theory, exhibit several of the qualitative features predicted by the model, show the separation capability of the device, and introduce a potentially versatile strategy for VC.

Consider the motion of noninteracting Brownian particles through a potential energy landscape $V(x, z)$ (periodic in x and invariant in y—see Fig. 1), and driven by a constant external force $\boldsymbol{F}$ [oriented at an angle $\theta_F = \arctan(F_y/F_x)$], with any vertical component conveniently incorporated into the potential V. The asymptotic distribution of particles in a unit cell is given by the steady-state

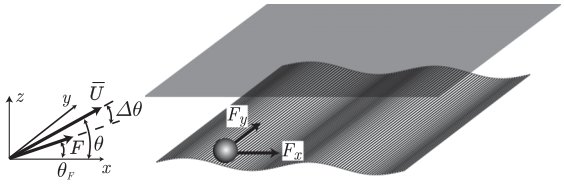

FIG. 1. Particle driven by a constant external force $\boldsymbol{F}$ in a fluidic device. The bottom surface, periodic in x and invariant in y, represents either the applied potential $V(x, z)$ at a given height z or the topography of the bottom wall. The forcing angle θ_F, the average velocity $\bar{\boldsymbol{U}}$, the migration angle θ, and the deflection angle $\Delta\theta$ are shown.

solution of the Smoluchowski equation for the *reduced* probability density $P^{\infty}(\boldsymbol{x})$ [18,19],

$$0 = \nabla \cdot \boldsymbol{J}(\boldsymbol{x}) = \nabla \cdot [\boldsymbol{U}(\boldsymbol{x})P^{\infty}(\boldsymbol{x}) - \boldsymbol{D}(\boldsymbol{x}) \cdot \nabla P^{\infty}(\boldsymbol{x})], \quad (1)$$

where $\boldsymbol{J}(\boldsymbol{x})$ is the probability density flux, $\boldsymbol{U}(\boldsymbol{x})$ is the instantaneous particle velocity, and $\boldsymbol{D}(\boldsymbol{x})$ is the diffusion tensor. In the low Reynolds number limit, the velocity of the particle is a linear combination of the forces acting on it, $\boldsymbol{U}(\boldsymbol{x}) = \boldsymbol{M}(\boldsymbol{x}) \cdot [\boldsymbol{F} - \nabla V(\boldsymbol{x})]$, where $\boldsymbol{M}(\boldsymbol{x})$ is the mobility tensor, which locally satisfies the Stokes-Einstein relation $\boldsymbol{D}(\boldsymbol{x}) = k_B T \boldsymbol{M}(\boldsymbol{x})$. $P^{\infty}(\boldsymbol{x})$ is periodic in x, satisfies the no-flux condition in z, and is normalized, $\int_{\tau} P^{\infty}(\boldsymbol{x}) dV = 1$, where τ is the volume of the unit cell. Given $P^{\infty}(\boldsymbol{x})$, it is straightforward to compute the components of the average velocity $\bar{U}_{x,y} = \int_{\tau} J_{x,y} d\tau$ [18] and the migration angle $\theta = \arctan(\bar{U}_y/\bar{U}_x)$, which is the relevant parameter in VC.

In planar microfluidic devices, the particles are usually highly confined in the vertical direction, either geometrically in narrow channels or due to particle-wall interaction potentials with narrow secondary minima [7,11,13]. In this case, the ratio between the diffusive time in the vertical direction and the transit time along a unit cell of the patterned surface is usually small, and it is valid to assume fast equilibrium in the cross section [13,20]. This is known as the Fick-Jacobs (FJ) approximation [3,21–23] and is analogous to other projection methods that eliminate fast degrees of freedom [24–26]. In this approximation, it is possible to write the probability distribution in terms of the marginal probability density, $\mathcal{P}(x)$, and the equilibrium conditional distribution in the cross section, $\rho(z|x)_{\text{eq}}$,

$$P^{\infty}(\boldsymbol{x}) \approx \mathcal{P}(x)\rho(z|x)_{\text{eq}} = \mathcal{P}(x)\mathcal{Q}^{-1}e^{-\beta V(x,z)}, \quad (2)$$

where $\beta = (k_B T)^{-1}$ and $\mathcal{Q}(x) = \int \exp[-\beta V(x,z)] dz dy$ is the local partition function. The average velocity in the invariant direction is then given by the average mobility, $\bar{U}_y = [\int_0^{\ell_x} \langle M^{yy} \rangle_{\text{eq}} \mathcal{P}(x) dx] F_y$, where M^{yy} is the hydrodynamic mobility and, for any function $f(x,z)$, $\langle f \rangle_{\text{eq}} = \int f(x,z)\rho(z|x)_{\text{eq}} dz dy$ is the local equilibrium average over the cross section. Before we calculate the average velocity in the periodic direction, we note that the total flux through any cross section in the periodic direction, $\mathcal{J}_x = \iint J_x dy dz$, is constant in the steady state and therefore $\bar{U}_x = \ell_x \mathcal{J}_x$. Integrating Eq. (1) over the cross section and using the FJ approximation, we obtain

$$\mathcal{J}_x = \langle M^{xx} \rangle_{\text{eq}} \left\{ [F_x - \mathcal{F}(x)]\mathcal{P} - k_B T \frac{d\mathcal{P}}{dx} \right\}, \quad (3)$$

where $\mathcal{F}(x)$ is the mean force due to the potential, and, following Zwanzig's approach to the case without convection [3], we write it in terms of the local free energy of the system, $\mathcal{A}(x) = -k_B T \ln \mathcal{Q}(x)$,

$$\mathcal{F}(x) = -\left\langle \frac{\partial V}{\partial x} \right\rangle_{\text{eq}} = -\frac{\partial \mathcal{A}(x)}{\partial x}. \quad (4)$$

It is clear from Eq. (3) that the total flux in the periodic direction, and therefore $\bar{U}_x$, have both diffusive and convective contributions. The first convective term shows that, as expected, a macroscopic anisotropy in the mobilities, $\langle M^{xx} \rangle_{\text{eq}} \neq \langle M^{yy} \rangle_{\text{eq}}$, could lead to a nonzero deflection angle, $\Delta\theta = \theta - \theta_F \neq 0$. Furthermore, the dependence of $\langle M^{xx} \rangle_{\text{eq}}$ on x can also result in $\Delta\theta \neq 0$, independent of the local isotropy of the mobility tensor, given that the contribution of the diffusive flux to $\bar{U}_x$ [last term in Eq. (3)] would not vanish in this case [13]. For simplicity, however, we shall assume that the mobility functions are constant and equal, $M^{xx} = M^{yy} = M$. In this case, we have $\bar{U}_y = MF_y$ and it is clear that $\Delta\theta \neq 0 \Leftrightarrow \bar{U}_x \neq MF_x$. Moreover, in this case, the diffusive contribution to $\bar{U}_x$ vanishes, and therefore only $\mathcal{F}(x)$ can contribute to a nonzero deflection angle. Solving Eq. (3) [13,24], we obtain

$$\tan\theta = \tan\theta_F \left[\frac{\text{Pe}}{1 - e^{-\text{Pe}}} \times \int_0^1 d\tilde{x} e^{-\beta \mathcal{A}'(\tilde{x})} \int_{\tilde{x}}^{\tilde{x}+1} d\xi e^{\beta \mathcal{A}'(\xi)} \right], \quad (5)$$

where $\beta \mathcal{A}'(\tilde{x}) = \beta \mathcal{A}(\tilde{x}) - \text{Pe}\tilde{x}$ and $\tilde{x} = x/\ell_x$. The Péclet number, $\text{Pe} = \beta F_x \ell_x$, compares the magnitudes of convective and thermal transport and is one of the dimensionless parameters dictating the migration angle. In general, one can use a characteristic value of the mean force, such as its maximum value $\mathcal{F}_{\text{max}}$, and consider the normalized driving force $f = F_x/\mathcal{F}_{\text{max}}$ as an independent parameter. In fact, we shall see below that Pe and f are complementary for the description of a given system, in that one is the appropriate parameter to consider when the other diverges. The other dimensionless number governing the migration angle is the partition ratio $\mathcal{K} = \exp(\beta \Delta \mathcal{A})$, where $\Delta \mathcal{A}$ is the amplitude of changes in the free energy over a unit cell. The partition ratio, which in the context of transition-state theory corresponds to an Arrhenius factor [27], measures the spatial variations in the equilibrium distribution of particles in a unit cell.

In Figs. 2 and 3, we investigate the effect of Pe and $\mathcal{K}$ on the deflection angle. We consider a *cosine* potential, $\tilde{\mathcal{A}}(\tilde{x}) = 1/2 \cos 2\pi\tilde{x}$, and a *dichotomous potential with linear transitions* (LTD potential), given by regions of constant potential, $\tilde{\mathcal{A}} = 0$ and $\tilde{\mathcal{A}} = 1$, and connected by linear transitions of width δ (see the inset in Fig. 3). The LTD potential in the limit $\delta = 0$ corresponds to a *square wave* (SW) potential. In all cases, the effect of the periodic potential is to reduce $\bar{U}_x$ [28], resulting in positive deflection angles (here, we consider $\theta_F = 45°$; thus, $0° < \Delta\theta \leq 45°$—see Fig. 1). In Fig. 2, we show the deflection angle as a function of Pe for the different potentials. It is clear that the deflection angle decreases with Pe and increases with $\mathcal{K}$ (arrow direction) independent of its entropic or energetic origin. Figure 2 also shows that, for a given $\mathcal{K}$ and Pe, the smaller the transition region in the LTD potential the higher the deflection angle, with $\Delta\theta$

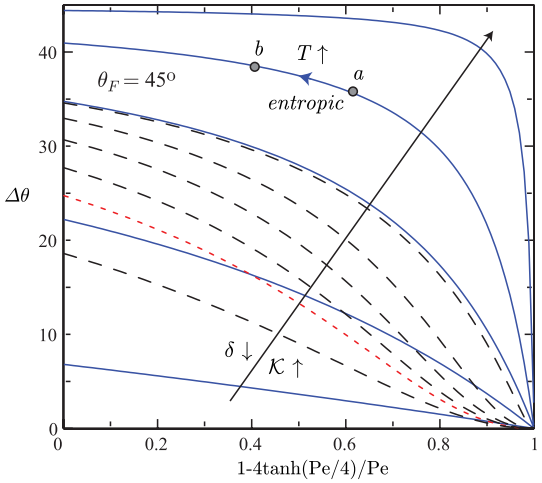

FIG. 2 (color online). Deflection angle as a function of Pe. Solid lines correspond to the SW potential with $\log\mathcal{K} = \beta\Delta\mathcal{A} = 1$, 2, 3, 4, and 6. The dashed lines correspond to the LTD potential with $\beta\Delta\mathcal{A} = 3$, transition regions $\delta = 0.01, 0.1, 0.2, 0.3, 0.5$, and $\epsilon_1 = \epsilon_2 = 0.5 - \delta$. The dotted line corresponds to the cosine potential. The arrow traverses curves of increasing $\mathcal{K}$ for the SW potential and curves of decreasing δ for the LTD potential. The evolution ($a \rightarrow b$) of a purely entropic system upon a temperature increase is shown.

converging to the curve for the SW potential as expected for $\delta \rightarrow 0$ (arrow direction). In Fig. 3, we plot the deflection angle as a function of the normalized force and consider the effect of Brownian motion for the different potentials. Specifically, we compare the deflection angle obtained at a finite partition ratio for the cosine and LTD potentials with that in the deterministic limit. [Note that

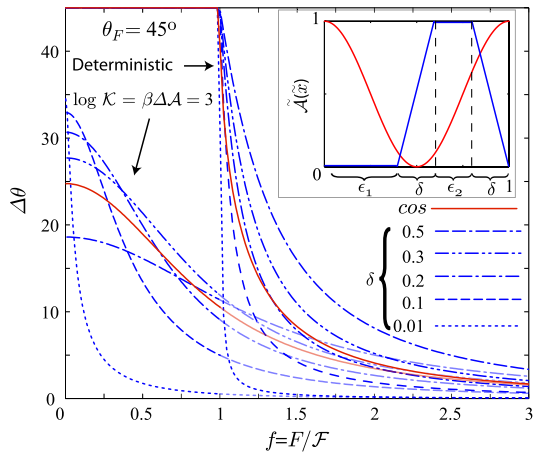

FIG. 3 (color online). Deflection angle as a function of the normalized force in the stochastic and deterministic regimes. The solid lines correspond to the cosine potential, while the dashed lines correspond to the LTD potential for different transition regions, and $\epsilon_1 = \epsilon_2 = 0.5 - \delta$. (Curves with the same δ have the same line style.) The inset shows schematics of the cosine and the LTD potentials.

Figs. 2 and 3 are complementary, in that they allow us to investigate independent limits, i.e., the SW limit where the opposing potential force is much larger than the driving force ($f \rightarrow 0$ and finite Pe) and the deterministic limit (Pe $\rightarrow \infty$ and finite f), respectively.] In all cases, the deflection angle decreases with f, analogous to the behavior observed in Fig. 2 for increasing Pe. Figure 3 also shows that Brownian motion allows the particles to cross the potential barriers when $f \leq 1$, leading to $\Delta\theta < 45°$ for all driving forces. This is in contrast to the deterministic case, in which particles are locked to move along the invariant direction and $\Delta\theta = 45°$ for $f \leq 1$. We also investigate the effect that the transition region δ has on the deflection angle. In the deterministic limit, the deflection angle for the LTD potential has the simple analytical expression [20]

$$\frac{\tan\theta}{\tan\theta_F} = \left[1 - 2\delta + \frac{f\delta}{f-1} + \frac{f\delta}{f+1}\right] = \left[1 + \frac{2\delta}{f^2-1}\right], \tag{6}$$

and it is clear that larger transition regions lead to larger deflection angles for any $f > 1$. The reason is that, as δ increases (at constant f), the particle is deflected for a longer time as it crosses the potential barrier. Note the different transit times coming from the regions with $\pm f$, as shown by the corresponding terms in Eq. (6). In the presence of Brownian motion, we observe the same trend for large driving forces f, as expected. On the other hand, as the driving force decreases and barrier hopping is dominated by thermal motion, the behavior reverses and larger transition regions lead to smaller deflection angles. This crossover between the deterministic and Brownian cases as f decreases is consistent with the behavior observed as a function of Pe in Fig. 2. In fact, the limits Pe $\ll 1$ and $f \ll 1$ correspond to the linear response regime, where the reduction in mobility (and effective diffusivity) is given by $\int \mathcal{Q}\,dx \int \mathcal{Q}^{-1}\,dx$ [29]. In Fig. 4, we show the effect of the partition ratio on the deflection angle for the LTD potential with a given δ. Clearly, the deflection angle increases with the partition ratio, converging to an asymptotic curve for $\mathcal{K} \rightarrow \infty$. This upper limit coincides with the deterministic limit for a purely energetic potential of mean force [9]. In terms of separation devices, it is then clear that, in order to obtain large deflection angles and high selectivity, it is desirable to operate around $f \lesssim 1$. The results presented in Figs. 2 and 4 also reveal the role of temperature in different separation systems [5]. In entropic trapping, for example, $\Delta\mathcal{A} \propto 1/\beta$, which implies that $\mathcal{K}$ is completely determined by the ratio between the available configurations in the slit and well regions, independent of the temperature [8]. On the other hand, both Pe and f decrease with temperature, which, in Figs. 2 and 4, corresponds to the system moving along curves of constant $\mathcal{K}$ towards higher discrimination angles, as shown. In contrast, in the purely energetic case, both $\Delta\mathcal{A}$ and f

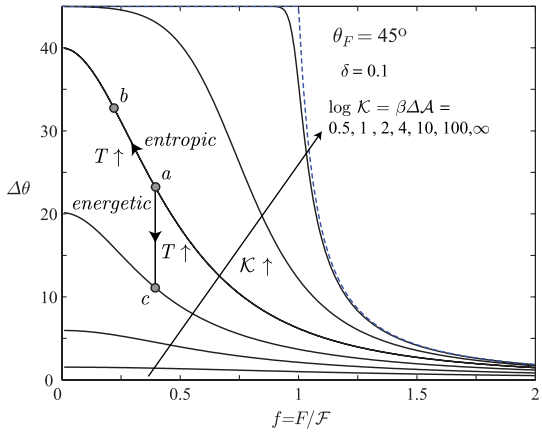

FIG. 4 (color online). Deflection angle as a function of the normalized force for the LTD potential for different partition ratios. The arrow traverses curves of increasing partition ratio. $\epsilon_1 = \epsilon_2 = 0.4$. $\delta = 0.1$. The dashed curve corresponds to the deterministic limit. $a \rightarrow b$ ($a \rightarrow c$) represents the evolution of a purely entropic (energetic) system upon a temperature increase.

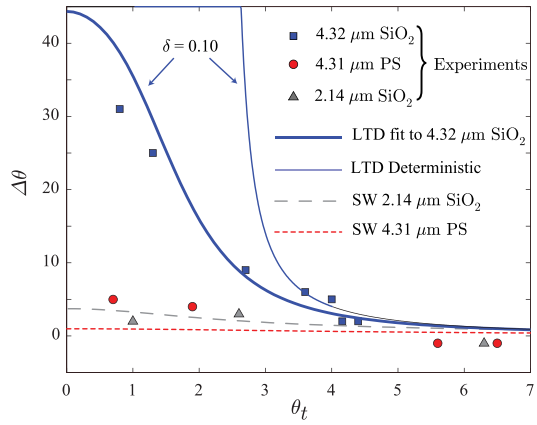

FIG. 5 (color online). Deflection angle as a function of the tilt angle. The solid symbols correspond to the experimental data as indicated. The dashed and dotted lines correspond to the SW potential. The solid curves correspond to a fit with a LTD potential using the width of the transition region as a fitting parameter ($\delta = 0.10$). See the Supplemental Material for the standard deviations and for a video showing a representative experiment with 4.32 μm silica particles [20].

are independent of temperature, and thus increasing the temperature reduces the partition ratio and the deflection angle, which corresponds to a system moving down along vertical lines of constant f in Fig. 4, as shown.

We also performed experiments in a microfluidic system in which suspended particles [silica (SiO_2) particles of 4.32 and 2.14 μm diameter and polystyrene (PS) particles of 4.31 μm diameter] are driven over a periodic array of parallel grooves etched in glass. (The shallow grooves are $\Delta\mathcal{H} = 65$ nm deep and 13 μm wide. $\ell_x = 20$ μm.) The separation between the channel walls is large enough to neglect confinement effects. Gravity induces periodic energy barriers due to the presence of the grooves and also drives the particles (the bottom surface is tilted at an angle θ_t). The gravity-induced partition ratio for a particle of radius a is given by $\mathcal{K} = \exp(4/3\pi a^3 \Delta\rho g \cos\theta_t \Delta\mathcal{H}/k_B T)$, where $\Delta\rho$ is the buoyant density of the particles and g is the acceleration due to gravity [13]. In a horizontal device, the partition ratio of the 4.32 μm silica particles is at least 2 orders of magnitude larger than that for either the smaller silica or the lighter polystyrene particles. Thus, at small tilt angles, the 4.32 μm silica particles should experience much larger deflections than the other particles, which would demonstrate that it is possible to fractionate particles by size or density. In Fig. 5, we show the measured deflection angle (for $\theta_F = 45°$) as a function of the tilt angle (note that, unlike Pe and f, θ_t is common to all particles in a given experiment). The thick solid line corresponds to the LTD potential, with δ calculated from the best fit to the experimental data and representing an effective transition region in the interaction between a suspended particle and the bottom grooves. We obtain good agreement for the 4.32 μm silica particles with $\delta = 0.10 \pm 0.01$ (2.0 ± 0.2 μm), which compares well with an order-of-magnitude estimate $\delta_{\mathrm{zoi}} = 2\sqrt{2(a + h_e)(\Delta\mathcal{H} + \kappa^{-1})} = 1.4$ μm obtained by extending the concept of a *zone of influence* [30] for a particle suspended at its equilibrium separation from the wall ($h_e = 259$ nm) and in the vicinity of a step [20]. The good agreement between the experiments and the analysis based on the FJ approximation, even at relatively large Pe, results from the narrow confinement of the particles by the effective particle-wall interaction potential, which considerably reduces the diffusive equilibration time in the cross section [20]. In Fig. 5, we also compare the results with the deterministic curve for the LTD potential with the same $\delta = 0.10$ (thin solid line). The clear deviation from experiments for $f \leq 1$ highlights the role of Brownian motion reducing the deflection angle. The theoretical curves for 2.14 μm silica and 4.31 μm polystyrene particles are insensitive to the width of the transition region, with differences smaller than 2.5°, and the data are compared to SW potentials, with good agreement. In these latter cases, the particles easily overcome the energy barriers due to thermal fluctuations, significantly reducing confinement effects and leading to small deflection angles.

We presented a unified description of planar vector chromatography in terms of the 1D periodic free energy of the system, including both energetic and entropic contributions, that encompasses the deterministic and stochastic limits. This description highlights the key parameters governing the migration angle of different species. We performed experiments in which gravity, along with a bottom surface patterned with slanted periodic grooves, can be used to separate particles according to their mass, in agreement with our analysis. More generally, other

fields, e.g., electric, dielectrophoretic, or magnetic, can play or enhance the role of gravity, potentially leading to a versatile technique.

The authors thank Professor Asthagiri for helpful discussions and Carson T. Riche for his assistance during the initial stages of the project. This material is based upon work partially supported by the National Science Foundation under Grant No. CBET-0954840 and by the NIH under Grant No. U54CA143868.

*jbernate@jhu.edu
†drazer@jhu.edu

[1] J. Han and H. G. Craighead, Science **288**, 1026 (2000).
[2] J. Rousselet, L. Salome, A. Ajdari, and J. Prost, Nature (London) **370**, 446 (1994).
[3] R. Zwanzig, J. Phys. Chem. **96**, 3926 (1992).
[4] D. Reguera and J. M. Rubí, Phys. Rev. E **64**, 061106 (2001).
[5] D. Reguera, G. Schmid, P. S. Burada, J. M. Rubí, P. Reimann, and P. Hänggi, Phys. Rev. Lett. **96**, 130603 (2006).
[6] E. Yariv and K. D. Dorfman, Phys. Fluids **19**, 037101 (2007).
[7] X. Wang and G. Drazer, Phys. Fluids **21**, 102002 (2009).
[8] K. D. Dorfman, Rev. Mod. Phys. **82**, 2903 (2010).
[9] M. Pelton, K. Ladavac, and D. G. Grier, Phys. Rev. E **70**, 031108 (2004).
[10] K. Ladavac, K. Kasza, and D. G. Grier, Phys. Rev. E **70**, 010901 (2004).
[11] X. Wang and G. Drazer, Phys. Fluids **22**, 122004 (2010).
[12] P. S. Burada and G. Schmid, Phys. Rev. E **82**, 051128 (2010).
[13] J. A. Bernate and G. Drazer, J. Colloid Interface Sci. **356**, 341 (2011).
[14] K. D. Dorfman and H. Brenner, J. Colloid Interface Sci. **238**, 390 (2001).
[15] J. G. Kralj, M. T. W. Lis, M. A. Schmidt, and K. F. Jensen, Anal. Chem. **78**, 5019 (2006).
[16] D. W. Inglis, R. Riehn, R. H. Austin, and J. C. Sturm, Appl. Phys. Lett. **85**, 5093 (2004).
[17] C. Liu, T. Stakenborg, S. Peeters, and L. Lagae, J. Appl. Phys. **105**, 102014 (2009).
[18] H. Brenner and D. A. Edwards, *Macrotransport Processes* (Butterworth-Heinemann, Boston, 1993).
[19] Z. Li and G. Drazer, Phys. Rev. Lett. **98**, 050602 (2007).
[20] See Supplemental Material at http://link.aps.org/supplemental/10.1103/PhysRevLett.108.214501 for the analytical expression for the trajectory angle for the LTD potential in the Brownian case, for a description of the experimental system and methods, for details regarding the order-of-magnitude estimation of the width of the effective transition region and the validity of the FJ approximation, and for a video of a representative experiment with the 4.32 μm silica particles.
[21] M. H. Jacobs, *Diffusion Processes* (Springer, New York, 1967).
[22] P. S. Burada, G. Schmid, D. Reguera, J. M. Rubí, and P. Hänggi, Phys. Rev. E **75**, 051111 (2007).
[23] N. Laachi, M. Kenward, E. Yariv, and K. D. Dorfman, Europhys. Lett. **80**, 50 009 (2007).
[24] H. Risken, *The Fokker-Planck Equation: Methods of Solutions and Applications* (Springer, Berlin, 1989).
[25] R. Zwanzig, *Nonequilibrium Statistical Mechanics* (Oxford University Press, New York, 2001).
[26] P. Kalinay and J. K. Percus, J. Chem. Phys. **122**, 204701 (2005).
[27] P. Hänggi, P. Talkner, and M. Borkovec, Rev. Mod. Phys. **62**, 251 (1990).
[28] P. Reimann, Phys. Rep. **361**, 57 (2002).
[29] P. E. Parris, M. Kuś, D. H. Dunlap, and V. M. Kenkre, Phys. Rev. E **56**, 5295 (1997).
[30] N. Kozlova and M. M. Santore, Langmuir **22**, 1135 (2006).